# Handheld probe integrating laser diode and ultrasound transducer array for ultrasound/photoacoustic dual modality imaging

**K. Daoudi,[1,5,6] P.J. van den Berg,[1,5] O. Rabot,[2] A. Kohl,[2] S. Tisserand,[3] P. Brands,[4] and W. Steenbergen[1,*]**

[1]*Biomedical Photonic Imaging Group, MIRA Institute for Biomedical Technology and Technical Medicine, University of Twente, PO Box 217, 7500 AE Enschede, The Netherlands*
[2]*Quantel Laser Diode, 2 bis Avenue du Pacifique, ZA de Courtaboeuf, 91940 Les Ulis, France*
[3]*SILIOS Technologies, Z.I Peynier-Rousset, Rue Gaston Imbert prolongée, 13 790 Peynier, France*
[4]*ESAOTE Europe, BV, P.O. Box 1132, 6201 BC, Maastricht, The Netherlands*
[5]*Contributed equally to the work*
[6]*k.daoudi@utwente.nl*
[*]*w.steenbergen@utwente.nl*

**Abstract:** Ultrasound and photoacoustics can be utilized as complementary imaging techniques to improve clinical diagnoses. Photoacoustics provides optical contrast and functional information while ultrasound provides structural and anatomical information. As of yet, photoacoustic imaging uses large and expensive systems, which limits their clinical application and makes the combination costly and impracticable. In this work we present and evaluate a compact and ergonomically designed handheld probe, connected to a portable ultrasound system for inexpensive, real-time dual-modality ultrasound/photoacoustic imaging. The probe integrates an ultrasound transducer array and a highly efficient diode stack laser emitting 130 ns pulses at 805 nm wavelength and a pulse energy of 0.56 mJ, with a high pulse repetition frequency of up to 10 kHz. The diodes are driven by a customized laser driver, which can be triggered externally with a high temporal stability necessary to synchronize the ultrasound detection and laser pulsing. The emitted beam is collimated with cylindrical micro-lenses and shaped using a diffractive optical element, delivering a homogenized rectangular light intensity distribution. The system performance was tested in vitro and in vivo by imaging a human finger joint.



**OCIS codes:** (110.0110) Imaging systems; (170.0170) Medical optics and biotechnology; (170.5120) Photoacoustic imaging.

## References and links

1. M. H. Xu and L. H. V. Wang, "Photoacoustic imaging in biomedicine," Rev. Sci. Instrum. **77**(4), 041101 (2006).
2. M. Heijblom, D. Piras, W. Xia, J. C. G. van Hespen, J. M. Klaase, F. M. van den Engh, T. G. van Leeuwen, W. Steenbergen, and S. Manohar, "Visualizing breast cancer using the Twente photoacoustic mammoscope: What do we learn from twelve new patient measurements?" Opt. Express **20**(11), 11582–11597 (2012).
3. P. Beard, "Biomedical photoacoustic imaging," Interface Focus **1**(4), 602–631 (2011).
4. M. H. Xu and L. V. Wang, "Universal back-projection algorithm for photoacoustic computed tomography," Phys. Rev. E Stat. Nonlin. Soft Matter Phys. **71**(1), 016706 (2005).
5. D. A. Boas, D. H. Brooks, E. L. Miller, C. A. DiMarzio, M. Kilmer, R. J. Gaudette, and Q. Zhang, "Imaging the body with diffuse optical tomography," Ieee Signal Proc. Mag. **18**(6), 57–75 (2001).
6. J. G. Fujimoto, "Optical coherence tomography for ultrahigh resolution in vivo imaging," Nat. Biotechnol. **21**(11), 1361–1367 (2003).
7. R. G. M. Kolkman, P. J. Brands, W. Steenbergen, and T. G. van Leeuwen, "Real-time in vivo photoacoustic and ultrasound imaging," J. Biomed. Opt. **13**(5), 050510 (2008).
8. J. J. Niederhauser, M. Jaeger, R. Lemor, P. Weber, and M. Frenz, "Combined ultrasound and optoacoustic system for real-time high-contrast vascular imaging in vivo," Ieee T Med. Imaging **24**(4), 436–440 (2005).

#221339 - $15.00 USD Received 20 Aug 2014; revised 6 Oct 2014; accepted 6 Oct 2014; published 17 Oct 2014

9. C. Haisch, K. Eilert-Zell, M. M. Vogel, P. Menzenbach, and R. Niessner, "Combined optoacoustic/ultrasound system for tomographic absorption measurements: possibilities and limitations," Anal. Bioanal. Chem. **397**(4), 1503–1510 (2010).
10. P. N. T. Wells, "Ultrasound imaging," Phys. Med. Biol. **51**(13), R83–R98 (2006).
11. C. Kim, T. N. Erpelding, L. Jankovic, M. D. Pashley, and L. V. Wang, "Deeply penetrating in vivo photoacoustic imaging using a clinical ultrasound array system," Biomed. Opt. Express **1**(1), 278–284 (2010).
12. T. J. Allen and P. C. Beard, "Pulsed near-infrared laser diode excitation system for biomedical photoacoustic imaging," Opt. Lett. **31**(23), 3462–3464 (2006).
13. R. G. M. Kolkman, W. Steenbergen, and T. G. van Leeuwen, "In vivo photoacoustic imaging of blood vessels with a pulsed laser diode," Lasers Med. Sci. **21**(3), 134–139 (2006).
14. M. Jaeger, S. Schupbach, A. Gertsch, M. Kitz, and M. Frenz, "Fourier reconstruction in optoacoustic imaging using truncated regularized inverse k-space interpolation," Inverse Probl. **23**(6), S51–S63 (2007).

## 1. Introduction

During last decades, the field of biomedical imaging has witnessed an emerging technique called photoacoustics [1–3] that is making its way towards clinical applications. In photoacoustic imaging, a short pulse of light is absorbed by tissue chromophores, which induces a local instantaneous temperature rise. The volume containing the chromophore instantaneously expands and consequentially builds up a pressure, which leads to the emission of an ultrasound wave. This wave can be detected with an ultrasound transducer array at the tissue surface. Then by knowing the sound propagation characteristics, the origin of the pressure wave can be traced back [4]. The spatial resolution is governed by the laser pulse duration and the bandwidth of the ultrasound probe, and the amplitude of the pressure wave is proportional to the absorbed energy density.

The excitement around photoacoustics is due to several important reasons. While commonly used optical techniques, such as diffuse optical tomography [5] and optical coherence tomography [6], suffer either from poor resolution or limited penetration depth due to the scattering nature of human tissues, photoacoustics combines high penetration depth and sub-millimeter ultrasound resolution, thanks to the weak ultrasonic scattering in biological soft tissues. Photoacoustics can be used to identify different functional activities of tissues by visualizing the presence of small blood vessels, the content of hemoglobin and its degree of oxygenation. Moreover, the ultrasound transducer arrays used in photoacoustic detection have also facilitated its combination with ultrasound pulse echo for dual modality imaging [7–9]. This association allowed to achieve valuable results, since ultrasound can provide complementary information, such as anatomy and structures, deep inside the interrogated medium with a likewise sub-millimeter resolution [10]. Until now, bulky lasers were used, making the proposed dual modality imaging systems large, costly, and with low frame rate imaging, complicating their clinical integration [11]. There is a growing need to develop photoacoustic imaging systems (PAI) that are compact, affordable and offering real-time imaging which will contribute to make photoacoustics a standard technique for clinical applications such as breast tumor, melanoma imaging and rheumatoid arthritis.

In this work we present a cost-effective portable PAI system combining ultrasound and photoacoustic imaging modalities. The PAI system takes advantage of the continuing development of efficient and cost-effective pulsed diode lasers and their use as a source for photoacoustics [12, 13]. In close collaboration with industrial partners (ESAOTE, Quantel and Silios) we developed a compact photoacoustic and ultrasound (PA/US) handheld probe, integrating an ultrasound transducer and a pulsed laser diode. The probe is used with a modified commercial portable ultrasound system for dual-modality imaging. The ultimate aim of the collaboration is to provide a portable real-time dual-modality imaging system which may help establishing photoacoustics as a routine instrument and offer more versatile tissue information. In the following sections we describe the dual-modality handheld probe and we evaluate the performance and feasibility of in-vivo measurements.

#221339 - $15.00 USD Received 20 Aug 2014; revised 6 Oct 2014; accepted 6 Oct 2014; published 17 Oct 2014

## 2. System development


Fig. 1. Portable imaging scanner combining photoacoustics and ultrasound, left is the ultrasound scanner system, right is the picture of the probe integrating laser module and ultrasound transducer array.

The main breakthrough of the proposed system is the miniaturization of the illumination system and its integration in the handheld probe. Figure 1 shows the developed imaging system combining photoacoustic and ultrasound imaging modalities. The system consists of two principal components: the commercial ultrasound scanner and the handheld probe integrating ultrasound detector, optical excitation and beam shaping systems.

### *2.1 Laser pulsing and beam shaping*

Figure 2 shows a schematic representation of the handheld probe. The probe was designed to fully integrate the ultrasound and illumination modules without exceeding a practical ultrasound probe size for the end user. We take advantage of the recent developments of diode laser technology, which has witnessed a tremendous improvement in efficiency and cost effectiveness. In this project we used a laser module specifically developed by Quantel (Paris, France). The emitting source consists of highly efficient diode arrays (Osram, Regensburg, Germany) mounted in a stack and emitting at 805 nm wavelength. The diodes are driven by a customized laser driver (Brightloop, France), allowing a pulse width of 130 ns at half maximum and a maximum 10 kHz pulse repetition rate. The driver can be triggered by an external trigger with high temporal stability, which is of utmost importance to synchronize the ultrasound detection and laser pulsing. The total delivered energy is around 0.56 mJ per pulse. The efficiency of the driver is around 60% and the total heat dissipation in the probe is about 36%. To limit the heat increase an aluminum rim is added to the design to provide cooling of the diode array and driver via air or operator's hand.

#221339 - $15.00 USD Received 20 Aug 2014; revised 6 Oct 2014; accepted 6 Oct 2014; published 17 Oct 2014

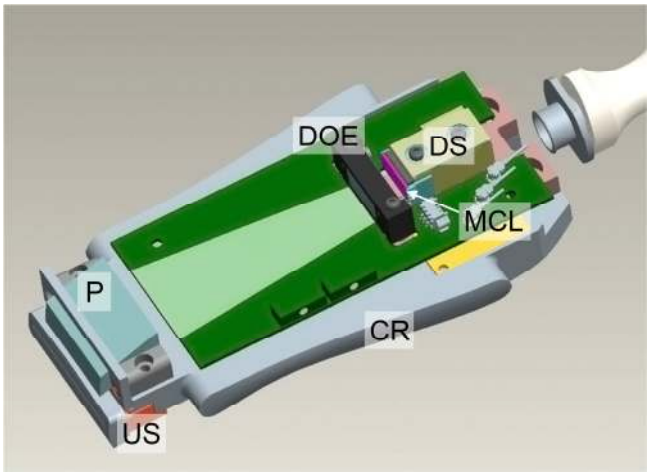


Fig. 2. A schematic of the handheld probe. US: ultrasound array transducer, P: deflecting prism, DOE: diffractive optical elements, DS: diode stack, MCL: micro-cylindrical lenses, CR: Aluminum cooling rim.

Light emitting from typical diode lasers suffers from bad beam quality with divergence angle much bigger than that of conventional lasers. The divergence is very pronounced, with angles of up to 40 degrees in the axis perpendicular to the diode arrays ('fast axis') and 10 degrees in the parallel axis ('slow axis') at Full Width Half Maximum (FWHM). It results in a rapidly expanding elliptical cone beam. Therefore, it is important to collimate and shape the laser beam to minimize energy loss and to illuminate the region of interest with a desired beam profile. There are different ways to reshape diode beams, and we opted for combination of cylindrical lenses and diffractive optical elements (DOE) provided by SILIOS Technologies (Peynier-Rousset, France). The DOEs can realize almost the same phase functions as refractive optics such as lenses, prisms or aspheres. They can also provide optical functions that are not achievable with conventional refractive optics because the phase function cannot be manufactured in a refractive way. Moreover, as the optical function is coded on the surface and not in the bulk part of the substrate, they are much smaller and lighter which is important for the miniaturization. In our system, the beam is first collimated by means of cylindrical micro-lenses placed in front of the diodes to minimize the divergence of the beam in the fast axis and allow beam shaping. Using a fused silica DOE composed of 400 μm diffractive cells and 8 discrete phase levels, the beam is homogenized in the fast axis and reshaped in rectangular form onto the skin. The DOEs designed for our shaping system shows an efficiency of 80%. The optical system is mounted in front of the diode stack (see Fig. 2).

To ensure overlap between deep illuminated tissue volume and the ultrasound detection plane, the medium will be illuminated under an angle. Monte Carlo simulations have shown that at targeted depths 5 to 10 mm, the fluence decreases by increasing the distance between the injection point and the ultrasound detection plane while the angle of illumination has less effect due to scattering. To optimize the fluence deep in tissue we need to minimize the distance between the injection point and ultrasound imaging plane by either minimizing the distance ultrasound-laser modules or by deflecting light with a large angle. The maximum angle of 51°, imposed by dimension limitations, allows an injection point at 2 mm from the ultrasound imaging plane when the skin is at 2 mm away from the probe. This angle will also allow the user to fine-tune the injection point by slightly varying the probe–skin distance. Around 5 mm distance the laser beam and ultrasound imaging plane are overlapping. In order to obtain the required beam deflection, a prism was designed and integrated into the probe (Fig. 2). By deflecting the light under an angle through a glass prism we also prevent

#221339 - $15.00 USD Received 20 Aug 2014; revised 6 Oct 2014; accepted 6 Oct 2014; published 17 Oct 2014

hazardous light emission when the probe is in contact with the air, thanks to the total internal reflection at the glass-air interface.

*2.2 Ultrasound detection and image reconstruction*

The ultrasound detection is performed with an ultrasound pulse/receiver array (based on the commercial Esaote SL3323 ultrasound probe) composed of 128 elements, each with a length of 5 mm and a pitch of 0.245 mm. The array has a central frequency of 7.5 MHz and a measured −6 dB bandwidth of around 100%. The array incorporates an acoustic lens to focus the ultrasound in the elevation plane at about 20 mm distance. The ultrasound module is separated from the laser system using electromagnetic shielding to prevent EM noise, which may be generated by the laser driver, from interfering with US detection. The probe is connected to a modified portable ultrasound scanner MyLab_One (ESAOTE Europe B.V, Maastricht, the Netherlands).

For the purpose of the project, the scanner underwent certain modifications to allow photoacoustic imaging: 1) providing an external signal to trigger the laser driver in order to synchronize between the detection and illumination, and 2) providing the possibility to block US transmission during photoacoustic measurements to allow switching between ultrasound and photoacoustic imaging, 3) modification of the ultrasound beam forming method. The commercial ultrasound scanner uses a standard line-by-line detection approach in combination with dynamic beam focusing and steering. Each pulse is used to build a line of the image and a full frame is generated from 128 pulses. Thus, to maintain real-time imaging of for example 25 images/sec without averaging, one will need a 4.2 kHz pulse repetition frequency (PRF). This PRF is possible since the ultrasound imaging system has a PRF of 12.8 kHz giving a maximum frame rate of 80 frames/sec. On the other hand photoacoustics uses laser pulses to interrogate the medium and the maximum permissible exposure (MPE), depending on the laser energy per pulse and laser PRF, restricts the illumination features. Therefore having 4200 pulses per second to obtain real time imaging will limit the maximum permissible energy to 0.01 mJ/cm$^2$. Hence, imaging through tissue will be a challenging task. Using advanced beam-forming of all elements and subsequent reconstruction instead of the line-by-line technique would allow high frame rate imaging with fewer pulses and therefore maintaining high pulse energy. The advanced beam-forming and reconstruction algorithm is not yet implemented onboard the MyLab_One in the current version of the system. Instead the scanner is connected to a laptop where RF data of all individual ultrasound elements are saved after being simultaneously acquired by the MyLab_One scanner with 50 MHz sampling frequency and digitized with a dynamic range of 12 bits. Afterwards, the data is reconstructed off-line using a Fourier reconstruction algorithm [14].

## 3. System performance

*3.1 Beam characteristics*

Figure 3 shows the laser beam intensity distribution at the front end of the probe, obtained by imaging the emitted beam at normal incidence 5 mm away from the probe using a CCD-based beam profiler with imaging optics. The image shows a rectangular beam shape spot with size at 1/e$^2$ of 17.6 mm horizontal to the ultrasound detector and 2.2 mm transversal to the probe. The profiles in both directions show a presence of a few peaks which will be of small effect in scattering media. The intensity variations were around ± 10% in a direction perpendicular to the beam, with approximately 8 lines/mm.

#221339 - $15.00 USD Received 20 Aug 2014; revised 6 Oct 2014; accepted 6 Oct 2014; published 17 Oct 2014

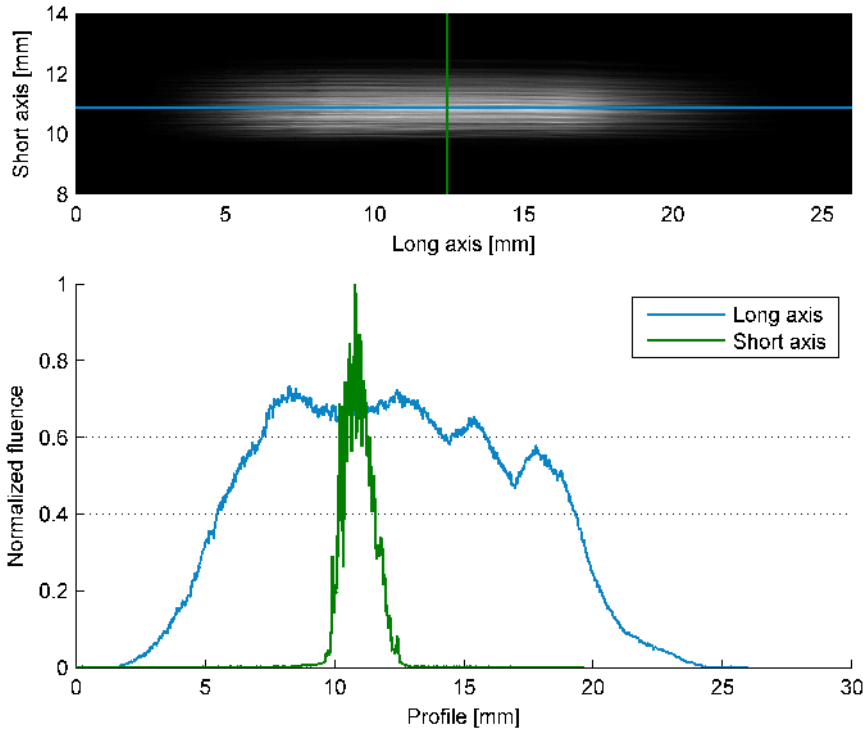


Fig. 3. Beam intensity distribution obtained 5 mm after the front-end of the handheld probe.

The energy delivered by the probe was measured using an integrating sphere and calorimeter. It was around 0.56 mJ per laser pulse corresponding to a total fluence of about 1.3 mJ/cm$^2$ of the angled beam on the skin. The stability of the laser energy was tested by measuring the pulse-to-pulse energy variation over a long period. A maximum variation of about 0.7% was found. The presence of the laser module in the handheld probe may cause an increase in local temperature of the probe. To evaluate this increase, direct measurements of temperature at different PRF were performed using a thermocouple positioned at the probe surface. The probe was in the air without any skin contact and measurements were done at laser side at different locations of the probe. Over ten minutes of laser firing at 2 kHz we only measured a slow increase of 3 degrees Celsius in the polymer casing and 7 degrees in the aluminum rim which will be drained out by the hand of the user. The temperature rise increases with pulse repetition frequency, and at 10 kHz we measured a rapid and more pronounced increase of 5-to-10 degrees in about 2 minutes of firing. However, the laser module will not be used at such PRF continuously due to the safety limitations related to the MPE.

#221339 - $15.00 USD Received 20 Aug 2014; revised 6 Oct 2014; accepted 6 Oct 2014; published 17 Oct 2014

*3.2 Photoacoustic resolution*

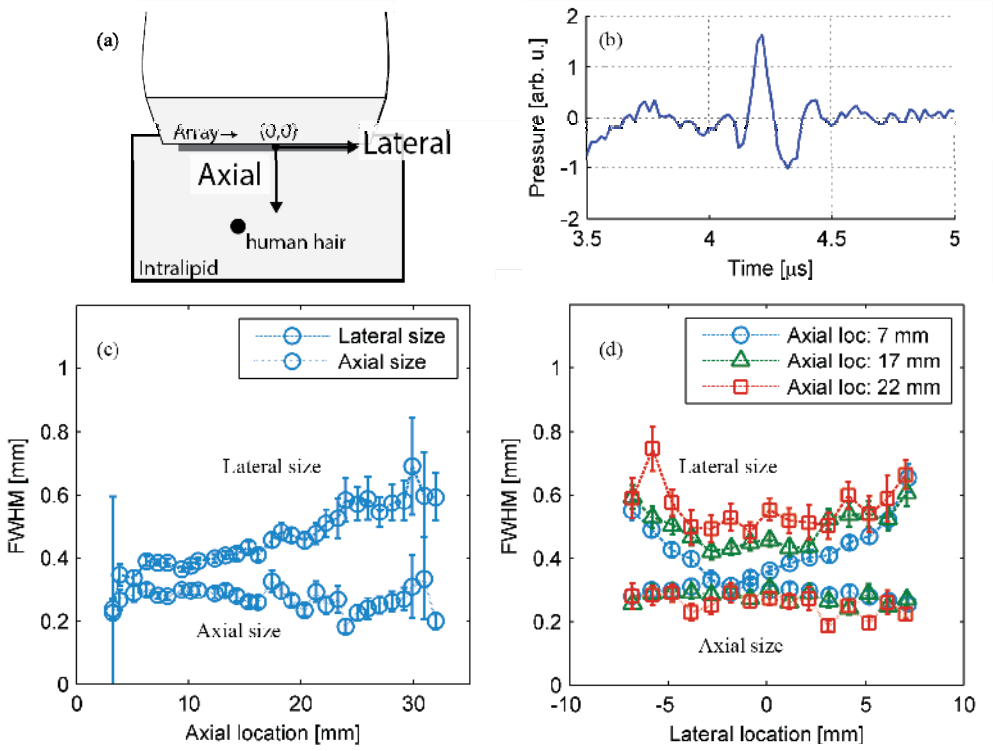


Fig. 4. Resolution estimation experiment, (a) schematic of the experimental set up, (b) (unreconstructed) time trace of a human hair, (c) resolution of reconstructed hair in lateral and axial axis at different depths, (d) axial and lateral resolution at different lateral positions for three depths (7 mm, 17 mm and 22 mm).

The resolution of the system was determined by measuring the PA point spread function using a black human hair of 80-85 μm diameter. The hair was placed in a bath containing water mixed with Intralipid to obtain a scattering medium of $\mu_s' = 3$ / cm (see Fig. 4(a)). The hair was translated in different directions to evaluate the variation of the resolution as a function of the absorber position. Figure 4(b) displays an example of the obtained time traces of the hair. To estimate the resolution RF-data of PA signals at each position of the scan were recorded, filtered, reconstructed and Hilbert transformed and subsequently fitted with a 2D Gaussian function. The size of the Gaussian was expressed as the Full Width Half Maximum (FWHM) which defined the resolution of the system. Figure 4(c) shows the lateral and axial resolution obtained by placing the hair at the center of the probe and changing the depth. The lateral resolution obtained deteriorates with axial location, from a FWHM of around 0.4 mm at 3 mm away, to a FWHM of 0.6 mm at 30 mm distance. Figure 4(d) is obtained by scanning the hair parallel to the probe (off axis) at three different depths (7 mm, 17 mm and 22 mm). Close to the transducer the lateral resolution also degrades from 0.4 mm to 0.6 mm when moving off-axis. Both trends are likely caused by the reduction of numerical aperture of the probe while moving deep or away from the probe center. The axial resolution in both scans is fairly invariant to location with 0.28 mm on average.

#221339 - $15.00 USD Received 20 Aug 2014; revised 6 Oct 2014; accepted 6 Oct 2014; published 17 Oct 2014

*3.3 Penetration depth*

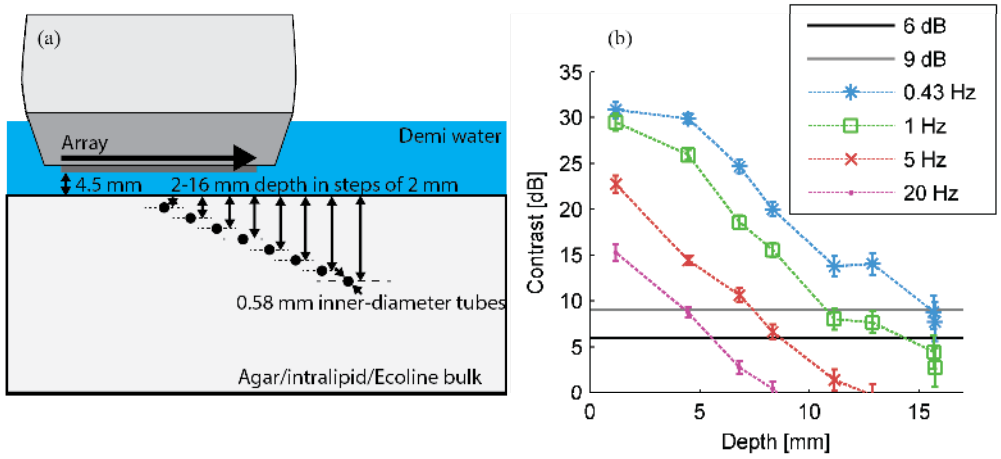


Fig. 5. (a) Schematic of the phantom used for the maximum depth experiments and (b) the contrast of the signal amplitude to the mean noise background as a function of depth and frame rate.

The maximum imaging depth of the system was measured in phantom experiments. The phantom used for these experiments consists of a bulk of Agarose gel with a mixture of Intralipid$^{20\%}$ and Ecoline black in water, leading to a tissue mimicking reduced scattering coefficient of 10 /cm and absorption coefficient of 0.03 /cm. Polyethylene tubing of 0.58 mm inner diameter was embedded at eight different depths (see Fig. 5(a)). Before measurements, the imaged tube is centered in the US field of view and filled with a 0.5% Ecoline black solution mimicking the absorption coefficient of blood: 4.2 /cm at 805nm while the other tubes are filled with water. 4000 photoacoustic frames (RF signals of all elements) are acquired at a PRF of 2 kHz and saved for offline processing. Before moving to the next tube, the current tube is flushed with water again.

Out of the 4000 photoacoustic frames, all, 500, 200, 43 or 10 are averaged, filtered and reconstructed, leading to image frame rates $f$ of 0.43 Hz, 1 Hz, 5 Hz and 20 Hz respectively. From these resulting images the contrast as a function of depth and frame rate is determined by considering the maximum peak at 1.5 × 1.5 mm$^2$ region around the tube to be the signal amplitude S and defining the mean noise level N in a 1.5 × 1.5 mm$^2$ region of interest 5 mm to the side of the tube. The contrast $C$ as a function of depth $d$ and frames $f$ is then given by:

$$C(d,f)=\frac{S(d)}{N(d,f)}.$$

The contrast converted to decibel is shown in Fig. 5(b). Lines of twice (6 dB) and three times (9 dB) the mean noise level were indicated in the graph as well: contrast values above these levels indicate where a tube is barely recognizable or is well visible respectively. Figure 5(b) shows how frame rate and imaging depth are interchangeable: by increasing the averaging at fixed PRF we improve the imaging depth but we decrease the imaging rate to remain under MPE. For real-time imaging (20 Hz, 10 averages) the imaging depth is fairly limited at 4-5 mm, while by lowering the frame rate to 5 Hz the depth can be increased to 7-8 mm. Moving to low frame rates like 1 Hz and 0.43 Hz penetration depths of 10 mm and 15 mm can be achieved respectively.

#221339 - $15.00 USD Received 20 Aug 2014; revised 6 Oct 2014; accepted 6 Oct 2014; published 17 Oct 2014

*3.4 In-vivo imaging*

The combined ultrasound and photoacoustic imaging was applied to one of the authors' index finger's proximal interphalangeal (PIP) joints to demonstrate the usability of the probe for in-vivo imaging. The Mylab_One was used with line by line mode for ultrasound detection and parallel mode for photoacoustic detection, such that each laser pulse provides a complete 2D image of the finger while 128 ultrasound pulses are used to reconstruct the ultrasound images. During the measurement, photoacoustic and subsequently ultrasound imaging modes were used with a corresponding acquisition of RF data. The switching between the two modes was done by changing the detection software in the MyLab FPGA. This caused a delay of 5 minutes between the acquisition of the US and PA images, where the subject tried to minimize positioning differences between the US and PA image. In the next version of the system both modes will be implemented together with reconstruction of parallel acquired signals within a GPU-based computation framework

The photoacoustic images are reconstructed from RF data that was averaged over 20 laser pulses to improve the signal to noise ratio. The MPE for the maximum possible fluence, 1.5 $mJ/cm^2$ when the laser beam is orthogonal to the skin, would allow for a continuous PRF of 210 Hz, giving a maximum imaging rate of 10 Hz. In these measurements a PRF of 1 kHz was used to reduce motion blur. Appropriate pauses were kept between the photoacoustic acquisitions to keep the average exposure below the MPE for non-uniform temporal exposure.

The index finger was positioned on an ergonomic support and submerged in water to facilitate easy translation of the probe and precise selection of the imaging plane. The measurements were performed with 4-5 mm distance between the probe and the skin for optimal illumination and to evade initial EM interferences which are present at the laser firing corresponding at 2 first mm in the image. At acquisition delay times corresponding to the > 3 mm imaging depths the initial interference was no longer present.

Combined PA/US images of the sagittal and transverse plane of the PIP joint are shown in Fig. 6. In these images the grayscale pixels correspond to US data whereas the heat-colored pixels correspond to PA data. The sagittal ultrasound image shows the skin and the underlying bone and joint gap. The transverse slice is located near the joint gap, showing bone, the skin and subcutaneous blood vessels. The photoacoustic images show the skin and blood vessels running parallel to the finger. The deeper photoacoustic signals correspond to the reflections of the PA signals on the bone.

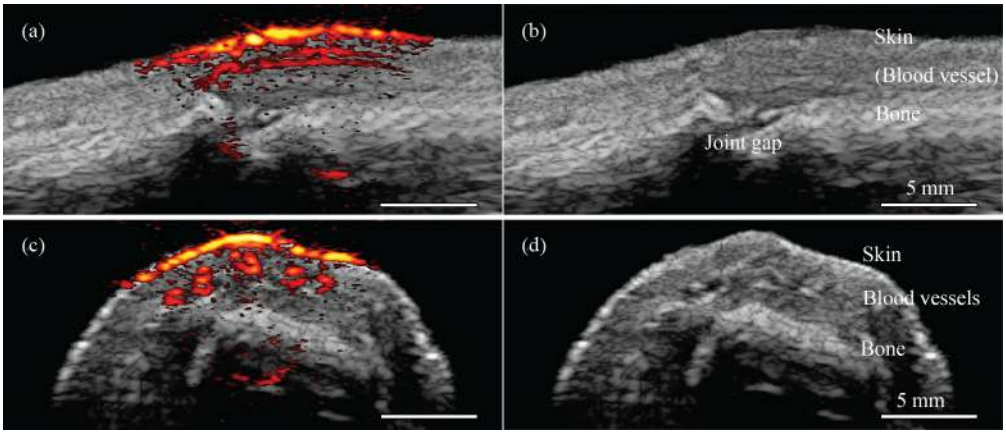


Fig. 6. Photoacoustic/ultrasound images of a human proximal interphalangeal joint in sagittal (a) and transverse (b) planes, with the upper part of the image corresponding to the dorsal side of the finger. On the right side, (b) and (c) show corresponding ultrasound only with anatomical structures indicated.

#221339 - $15.00 USD Received 20 Aug 2014; revised 6 Oct 2014; accepted 6 Oct 2014; published 17 Oct 2014

## 4. Discussion and conclusion

We presented a fully integrated handheld probe, combining an ultrasound array transducer and a diode laser module in a compact and ergonomic design. The first prototype presented in this work can achieve a laser fluence of up to 1.3 mJ/cm$^2$ on the skin with an illumination spot size of 18.2 × 2.3 mm$^2$. This was obtained by using stacked arrays of highly efficient diode lasers in combination with cylindrical micro-lenses and diffractive optical elements for beam shaping. The probe was used with a commercially available portable ultrasound scanner that was modified regarding the synchronization and detection to allow for photoacoustic imaging.

Phantom measurements showed a possible imaging depth of 10 to 15 mm for a frame rate of 0.5 Hz, while this depth is limited to 4 mm in real time imaging of 20 frames per second. This shallow imaging at high frame rate is dictated by the MPE regulations, which limit the PRF in relation to laser fluence. A possible measurement strategy would be to use a high frame rate PA imaging for selection of a field of view, after which the operator could acquire a single image with high imaging depth. Additionally we performed phantom experiments to estimate the axial and lateral resolution of the photoacoustic system at different locations. Results showed a lateral resolution of 0.4 mm which degrades to 0.6 mm with depth and the position off axis due to the limited numerical aperture, whereas the axial resolution in both scans was around 0.28 mm on average with negligible variation. The measured axial resolution agrees within 0.05 mm to the theoretical band limited resolution.

This resolution can be improved by decreasing the 130 ns pulse length of the current prototype. In fact, the resulting pressure wave in photoacoustic imaging can be seen as the photoacoustic signal (for a certain absorber size) convolved by the temporal pulse shape. Thus, the frequency content of the signal is directly related to the temporal width of the pulse. For longer pulses, higher frequencies are not generated which will reduce the resolution and decrease the sensitivity of the system to smaller blood vessels. We are currently investigating the possibility to decrease this pulse length in order to improve the image quality.

The designed probe was tested by performing in-vivo measurements on a healthy human finger joint. A co-registration of photoacoustic and ultrasound images was obtained. The ultrasound scanner system was used with parallel detection for photoacoustic imaging, giving a maximum achievable imaging rate of 10 images per second, while averaging over 20 frames per image. On the other hand ultrasound images were acquired using a standard line by line mode which can achieve 80 frames per second.

The system was used with two detection modes, line by line for US imaging and parallel detection mode for PA imaging. In the current study this was done consecutively by changing the scanner firmware. In the next version both modalities will be simultaneously available.

Concluding, a compact and handheld hybrid photoacoustic and ultrasound system has been presented. It has been successfully tested on a simple phantom and compared to beam profile data to confirm proper functioning. The study on a more complex phantom showed a penetration depth up to 15 mm for 0.5 Hz frame rate imaging, an axial resolution of 0.28 mm and lateral resolution ranging from 0.4 mm till 0.6 mm depending on the lateral position and depth. The hybrid probe has also been applied in vivo on a proximal interphalangeal joint of a healthy human subject, showing a detailed absorption distribution alongside the anatomical structure of the finger joint. The authors believe that the described system is a first step towards an affordable portable combined US-PA imaging system.

## Acknowledgment

Research was funded by the European Community's Seventh Framework Programme (FP7/2007-2013) under grant agreement n° 318067; by Agentschap NL under Eureka grant E!4993; and from the Technology Foundation in the Netherlands (STW) under Vici-grant 10831. Authors acknowledge Dr. M. Jaeger, Institute of Applied Physics, Bern University for providing software for the Fourier reconstruction algorithm.

#221339 - $15.00 USD Received 20 Aug 2014; revised 6 Oct 2014; accepted 6 Oct 2014; published 17 Oct 2014